Published OnlineFirst April 10, 2012; DOI: 10.1158/1078-0432.CCR-12-0445

Cancer Therapy: Preclinical

Clinical Cancer Research

Bridging the Gap between Preclinical and Clinical Studies Using Pharmacokinetic–Pharmacodynamic Modeling: An Analysis of GDC-0973, a MEK Inhibitor

Harvey Wong[1], Laurent Vernillet[2], Amy Peterson[3], Joseph A. Ware[2], Lillian Lee[5], Jean-Francois Martini[5], Peiwen Yu[5], Congfen Li[5], Geoffrey Del Rosario[5], Edna F. Choo[1], Klaus P. Hoeflich[4], Yongchang Shi[5], Blake T. Aftab[5], Ron Aoyama[5], Sanh Tan Lam[5], Marcia Belvin[4], and John Prescott[3]

Abstract

Purpose: GDC-0973 is a potent and selective mitogen-activated protein (MAP)/extracellular signal–regulated kinase (ERK) kinase (MEK) inhibitor. Pharmacokinetic–pharmacodynamic (PK–PD) modeling was used to relate GDC-0973 plasma and tumor concentrations, tumor pharmacodynamics and antitumor efficacy to establish pharmacokinetic endpoints and predict active doses in the clinic.

Experimental Design: A PK–PD model was used to characterize GDC-0973 tumor disposition and *in vivo* potency in WM-266-4 xenograft mice. Simulations were conducted using the PK–PD model along with human pharmacokinetics to identify a target plasma concentration and predict active doses. *In vivo* potency and antitumor efficacy were characterized in A375 melanoma xenograft mice, and a population-based integrated PK–PD-efficacy model was used to relate tumor pharmacodynamics (%pERK decrease) to antitumor activity.

Results: GDC-0973 showed a sustained tumor pharmacodynamic response due to longer residence in tumor than in plasma. Following single doses of GDC-0973, estimated *in vivo* IC_{50} values of %pERK decrease based on tumor concentrations in xenograft mice were 0.78 (WM-266-4) and 0.52 μmol/L (A375). Following multiple doses of GDC-0973, the estimated *in vivo* IC_{50} value in WM-266-4 increased (3.89 μmol/L). Human simulations predicted a minimum target plasma concentration of 83 nmol/L and an active dose range of 28 to 112 mg. The steep relationship between tumor pharmacodynamics (%pERK decrease) and antitumor efficacy suggests a pathway modulation threshold beyond which antitumor efficacy switches on.

Conclusions: Clinical observations of %pERK decrease and antitumor activity were consistent with model predictions. This article illustrates how PK–PD modeling can improve the translation of preclinical data to humans by providing a means to integrate preclinical and early clinical data. *Clin Cancer Res; 18(11); 3090–9. ©2012 AACR.*

Introduction

The RAF/MEK/ERK signaling pathway is highly conserved and plays an important role in cell proliferation, survival, migration, cell-cycle regulation, and angiogenesis (1–4). Activating mutations in B-RAF have been frequently observed in several tumor types, including 50% to 70% of malignant melanomas, 30% of papillary thyroid cancer, and 10% to 15% of colorectal and ovarian cancers, among others (1, 5–7). The majority of these mutations are in exon 15, which results in a Val^{600} Glu (V600E) amino acid substitution, leading to constitutive kinase activation (8). Cancer cells harboring the V600E B-RAF mutation have been shown to be particularly sensitive to inhibition of mitogen–activated protein (MAP)/extracellular signal–regulated kinase (ERK) kinase (MEK; ref. 9), making MEK an attractive target for small molecule inhibitors.

More than 10 MEK inhibitors have been evaluated in the clinic (4). Despite the activity around this target and signs of clinical efficacy (10, 11), none have yet been approved for clinical use. However, the recently approved B-RAF inhibitor, vemurafenib (PLX4032), has been reported to be very effective in patients with melanoma with mutated B-RAF causing robust complete or partial tumor regression (12).

Authors' Affiliations: Departments of [1]Drug Metabolism and Pharmacokinetics, [2]Clinical Pharmacology, [3]Exploratory Clinical Development, and [4]Cell Signaling Pathways, Genentech Inc.; and [5]Exelixis, South San Francisco, California

Note: Supplementary data for this article are available at Clinical Cancer Research Online (http://clincancerres.aacrjournals.org/).

Corresponding Author: Harvey Wong, Drug Metabolism and Pharmacokinetics, Genentech, Inc., 1 DNA Way, MS 412a, South San Francisco, CA 94080. Phone: 650-225-5739; Fax: 650-467-3487; E-mail: wong.harvey@gene.com

doi: 10.1158/1078-0432.CCR-12-0445

Published OnlineFirst April 10, 2012; DOI: 10.1158/1078-0432.CCR-12-0445

Translational Relevance

The current work applies pharmacokinetic–pharmacodynamic (PK–PD) modeling to characterize tumor disposition and pharmacodynamics of a mitogen-activated protein (MAP)/extracellular signal–regulated kinase (ERK) kinase (MEK) inhibitor, GDC-0973, in preclinical tumor models. PK–PD modeling was used to translate preclinical tumor accumulation characteristics and identify a minimum target plasma concentration in patients. Predictions of active doses were based upon $\geq$80% suppression of the RAF/MEK/ERK pathway and compared well with reported clinical responses. Using an integrated PK–PD efficacy model, the relationship between pathway modulation and efficacy was defined. Our analysis suggests a pathway suppression threshold beyond which antitumor activity switches on. Our observations are consistent with clinical data reported for PD-0325901, another MEK inhibitor, and vemurafenib, a B-RAF inhibitor, both of which target the RAF/MEK/ERK pathway. This work illustrates how PK–PD modeling can be used to improve the predictive value of preclinical data in the phase I setting.

The vemurafenib study highlights the importance of the RAF/MEK/ERK signaling pathway in cancers with B-RAF mutations. Therefore, it can be expected that there will be continued interest in MEK inhibitors as an alternative means of targeting the RAF/MEK/ERK pathway. Finally, MEK inhibitors given in combination with B-RAF inhibitors can provide a means to prevent the emergence of acquired drug resistance in tumors (13, 14).

GDC-0973 (also known as XL518), (*S*)-[3,4-difluoro-2-(2-fluoro-4-iodophenylamino)phenyl][3-hydroxy-3-(piperidin-2-yl)azetidin-1-yl]methanone (Supplementary Fig. S1), is a novel potent, selective MEK1 inhibitor with an IC_{50} estimate of 4.2 nmol/L in an *in vitro* biochemical assay against purified MEK1 enzyme (15). GDC-0973 showed more than 100-fold selectively for MEK1 over MEK2 and showed no significant inhibition when tested against a panel of more than 100 of serine-threonine and tyrosine kinases. Preliminary studies conducted in xenograft mice suggested that the duration of tumor phosphorylated ERK1/2 (pERK) inhibition, the predominant downstream measure of MEK inhibition, outlasted the presence of GDC-0973 in plasma, and was consistent with the residence time of GDC-0973 in tumors (data not shown). This observed disconnect between GDC-0973 plasma concentrations and tumor pharmacodynamic (PD) response suggested that additional investigation into the pharmacokinetic–pharmacodynamic (PK–PD) relationship of GDC-0973 in tumor was warranted.

Preclinical PK–PD modeling can play an important role in the drug discovery and development process by providing an integrated understanding of relationships between compound plasma concentrations, PD marker response, and efficacy. In addition, PK–PD modeling is a useful tool that can facilitate the translation of preclinical data to humans. The objectives of the current studies were (i) to characterize the tumor disposition and *in vivo* potency of GDC-0973 in xenograft mice, (ii) to estimate the minimum target GDC-0973 plasma concentrations in humans, and (iii) to characterize the relationship between RAF/MEK/ERK signaling pathway inhibition and antitumor efficacy. Our studies with GDC-0973 illustrate how the incorporation of early phase I clinical data into existing preclinical PK–PD models can serve not only to improve our understanding of the behavior of GDC-0973 in humans but also to help prospectively predict responses in the clinic.

Materials and Methods

GDC-0973 (also known as XL518; Supplementary Fig. S1) was provided by Exelixis. All studies were conducted using the dihydrochloride salt of GDC-0973. Solvents used for analysis were of analytic or high-performance liquid chromatography (HPLC) grade (Fisher Scientific). WM-266-4 and A375 human melanoma cells were purchased from American Type Culture Collection. All other reagents or material used in this study were purchased from Sigma-Aldrich unless otherwise stated. *In vivo* studies were conducted at Exelixis and the Exelixis Institutional Animal Care and Use Committee approved all procedures in animals.

In vivo PK–PD study in WM-266-4 xenografts

Briefly, 5 million WM-266-4 melanoma cells were resuspended in Hank balanced salt solution and implanted intradermally into the hind flank of female NCR nude mice (Taconic). On days 11 or 13 after the implantation, xenograft mice with tumor volumes of approximately 100 to 120 mm^3 were randomly assigned to 8 groups ($n = 27$ per group), 4 single dose groups and 4 multiple dose groups. One day after randomization and group assignment, mice in the single dose groups were given a single oral dose of vehicle (water for injection USP), 1, 3, or 10 mg/kg of GDC-0973 (expressed as free base equivalents). Mice in the multiple dose groups were given daily oral doses of vehicle (water for injection USP), 1, 3, or 10 mg/kg of GDC-0973 for 14 days. Plasma and tumor samples ($n = 3$ per time point) were collected from euthanized mice predose and at 2, 4, 8, 16, 24, 72, 120, and 168 hours postdose on day 1 (single dose groups) or day 14 (multiple dose groups). Samples were stored at −80°C until analysis. GDC-0973 concentrations in plasma and tumor lysates were determined using liquid chromatography/tandem mass spectrometry (LC/MS-MS). The dynamic range of the assay was 0.004 to 35 μmol/L. ERK1/2 phosphorylation was determined by Western blot analysis.

In vivo target modulation in A375 xenografts

A375 xenograft–bearing mice were established as described above for WM-266-4 xenograft–bearing mice. A375 xenograft–bearing mice were given a single oral dose of 0.3, 1, 3, 10, or 30 mg/kg of GDC-0973 (expressed as free

Published OnlineFirst April 10, 2012; DOI: 10.1158/1078-0432.CCR-12-0445

base equivalents). Plasma and tumor GDC-0973 concentrations and tumor pERK inhibition were assessed at 24 (all doses), 48 (10 and 30 mg/kg only), and 72 (10 and 30 mg/kg only) hours postdose ($n = 5$ animals per assessment). Quantitation of GDC-0973 concentrations in plasma and tumor and tumor %pERK decrease was conducted as described for the WM-266-4 studies.

Equation (D) was fit to GDC-0973 tumor concentrations and tumor %pERK decrease data from A375 xenografts using GraphPad Prism V4.02 (GraphPad Software Inc.). The Hill coefficient (h) was fixed to 1 for this analysis. The use of this model [Equation (D)] is explained in more detail in the PK–PD modeling section later.

In vivo efficacy study with A375 xenografts

The GDC-0973 *in vivo* efficacy study was conducted with A375 xenograft–bearing mice. Tumor volumes were measured in 2 dimensions (length and width) using Ultra Cal-IV calipers (Model 54-10-111, Fred V. Fowler Company, Inc.). The following formula was used with Excel v11.2 (Microsoft Corporation) to calculate tumor volume (TV): TV (mm^3) = (length × width^2) × 0.5. Tumors were monitored until they reached a mean volume of approximately 100 to 120 mm^3 at which time the mice were assigned to each dosing group ($n = 10$ animals per group) such that mean tumor volume was similar for each group. Mice in each group received oral doses of either vehicle (water for injection USP) once daily, 0.3 mg/kg once daily, 1 mg/kg once daily, 3 mg/kg once daily, 10 mg/kg once daily, 30 mg/kg every second day, or 30 mg/kg every third day of GDC-0973 free base equivalents for 14 days. Tumor sizes and body weights were recorded twice weekly, and the mice were regularly observed over the course of the study. Mice were euthanized if their tumor volume exceeded 2,000 mm^3 or if their body weight dropped by more than 20% of the starting weight.

PK–PD modeling

WM-266-4 xenograft PK–PD model. PK–PD modeling for the WM-266-4 xenograft studies was conducted using SAAM II (Saam Institute, University of Washington, Seattle, WA). Briefly, Equations (A) to (C) and Fig. 1A describe the PK model that was simultaneously fit to mean plasma and tumor GDC-0973 concentrations from single and multiple dose WM-266-4 xenograft mice studies. Equations (A) to (C) are described as follows:

$$\frac{dX_0}{dt} = -k_a X_0 \quad \text{(A)}$$

$$\frac{dC_p}{dt} = k_a X_0 + \mathrm{Cl_{tp}} C_t - \mathrm{Cl_{pt}} C_p - \mathrm{Cl} C_p \quad \text{(B)}$$

$$\frac{dC_t}{dt} = \mathrm{Cl_{pt}} C_p - \mathrm{Cl_{tp}} C_t, \quad \text{(C)}$$

X_0 (μmol/L) is the amount of GDC-0973 in the oral compartment, t (day) is time, k_a (day^{-1}) is the absorption rate constant, C_p (μmol/L) is the plasma GDC-0973 concentration, C_t (μmol/L) is the tumor GDC-0973 concentration, Cl (L/d/kg) is the plasma clearance, $\mathrm{Cl_{pt}}$ (L/d/kg) is the intercompartmental clearance from the plasma to the tumor compartment, and $\mathrm{Cl_{tp}}$ (L/d/kg) is the intercompartmental clearance from tumor to plasma compartment.

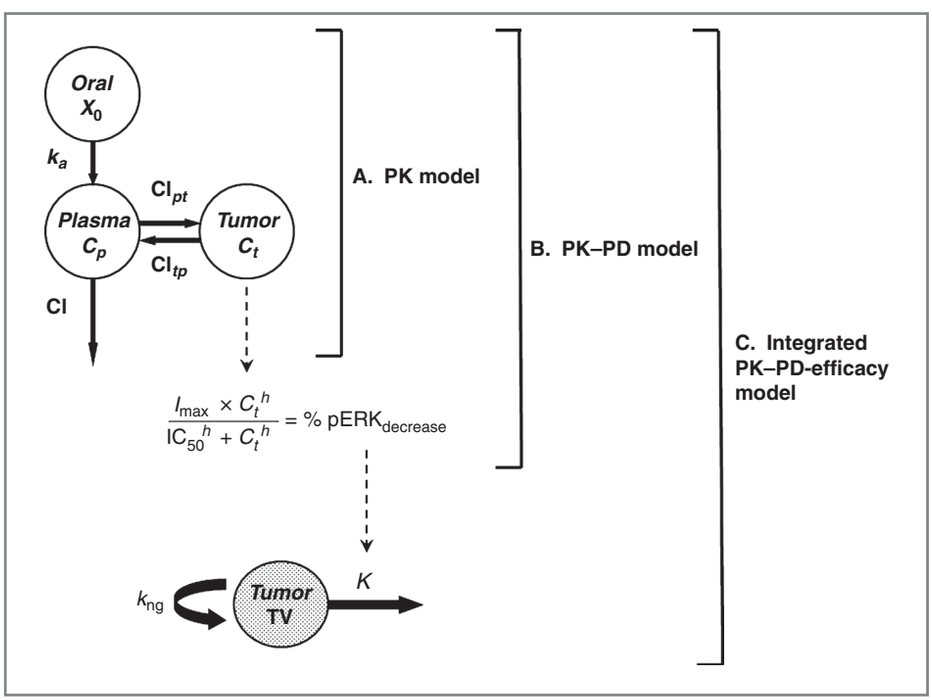

Figure 1. Models used in the analyses conducted in this article. A, the PK model describing tumor disposition of GDC-0973. B, the PK–PD model linking %pERK decrease in tumor to GDC-0973 tumor concentrations. C, an integrated PK–PD-efficacy model where the antitumor efficacy is driven by %pERK decrease in tumor.

Published OnlineFirst April 10, 2012; DOI: 10.1158/1078-0432.CCR-12-0445

The PD effect (%pERK decrease) was related to GDC-0973 tumor concentrations using the following equation:

$$\%\text{pERK}_{\text{decrease}} = \frac{\text{I}_{\max} \times C_t^h}{\text{IC}_{50}^h \times C_t^h} \quad \text{(D)}$$

Where $\%\text{pERK}_{\text{decrease}}$ (%) is the percentage decrease of pERK, $I_{\max}$ (%) is the maximum percentage decrease of pERK, h is the Hill coefficient, and IC_{50} (μmol/L) is the tumor concentration at which the $\%\text{pERK}_{\text{decrease}}$ is half of $I_{\max}$. Parameter estimates from the PK model described by Equations (A) to (C) were fixed before estimating the PD parameters shown in Equation (D). The PK–PD model [Equations (A)–(D) and Fig. 1B] was fit to %pERK decrease data from single and multiple dose studies separately as there were apparent changes in the tumor %pERK response to GDC-0973 following multiple days of dosing. PK and PD parameters estimates are presented as the estimate followed by the %SE in parentheses. Finally, the rationale for using the PK–PD model described by Equations (A) to (D) and Fig. 1B stemmed from observations from preliminary studies that the duration of tumor %pERK decrease was substantially longer than the presence of GDC-0973 in plasma and was consistent with the longer residence time of GDC-0973 in tumors.

Human simulations. Patients in the phase I clinical trial were given daily oral doses of GDC-0973 continuously for 21 days over a 28-day cycle (16). Mean GDC-0973 concentration–time data were obtained from 3 patients from cohort 1 who were given 0.05 mg/kg daily oral doses of GDC-0973 (16). In these 3 patients, plasma samples for PK evaluation were collected on days 1 and 21 at predose, 0.5, 1, 2, 4, 8, 24, 48 (day 21 only), and 192 (day 21 only) hours postdose. The WM-266-4 PK model accounting for tumor disposition described by Equations (A) to (C) and Fig. 1A was fit to mean human GDC-0973 concentration–time data to estimate Cl, k_a, and V/F (apparent volume of distribution in L/kg). Tumor disposition was assumed to be similar between humans and WM-266-4 xenografts, thus Cl_{tp} and Cl_{pt} were fixed during the PK model fitting process. Human PK parameters are presented as the estimate followed by the %SE in parentheses. Human PK parameter estimates along with PD parameters ($I_{\max}$, IC_{50}, and h) from the single and multiple dose WM-266-4 xenografts studies were used in the PK–PD model (Fig. 1B) to conduct human simulations to provide a range of response.

Integrated PK–PD-efficacy modeling. To relate pathway modulation (expressed as tumor %pERK decrease) to antitumor effect, an integrated population-based PK-PD-efficacy model (Fig. 1C) was used to fit individual longitudinal tumor data from A375 melanoma xenograft efficacy studies. The following equations describe the model used.

$$\frac{d(\text{TV})}{\text{dt}} = k_{\text{ng}}(\text{TV}) - K(\text{TV}) \quad \text{(E)}$$

$$\text{where} \quad K = \frac{K_{\max} \times (\%\text{pERK}_{\text{decrease}})^n}{K(\%I)_{50}^n + (\%\text{pERK}_{\text{decrease}})^n}$$

TV (mm^3) is defined as the tumor volume, k_{ng} (day^{-1}) is the net growth rate constant, K (day^{-1}) is the rate constant describing the antitumor effect of GDC-0973, $K_{\max}$ (day^{-1}) is the apparent maximum value of K, $K(\%I)_{50}$ is defined as the %pERK decrease where K is 50% of $K_{\max}$, and n is the Hill coefficient.

Briefly, %pERK decrease in tumor was simulated for all dose levels and schedules of the A375 xenograft efficacy study during fitting process using the WM-266-4 xenograft PK–PD model and estimated PD parameters from the *in vivo* target modulation studies with A375 xenografts (see Fig. 4A). The S-ADAPT program, an augmented version of ADAPT II with population analysis capabilities (17, 18), was used to fit individual tumor volumes from all dose levels of the A375 xenograft efficacy study simultaneously. Intersubject variability was assumed to be log-normally distributed and fitted using an exponential variance model. Residual variability error was modeled using a proportional-additive error model. In cases where intersubject variance was small and could not be estimated reliably, the intersubject variance was fixed to 0.00001. Population PD parameter estimates are presented as the estimate followed by the %SE in parentheses.

Results

Studies in WM-266-4 xenografts

PK–PD model adequately characterizes GDC-0973 tumor accumulation and tumor PD response in WM-266-4 xenograft mice. The objective of this study was to characterize the concentration of GDC-0973 in plasma and tumor tissue, the PD response in tumor tissue, and the associated PK–PD relationships over time. WM-266-4 melanoma cells are PTEN-deficient and harbor a V600D B-RAF mutation conferring activation of the RAF/MEK/ERK pathway that is functionally similar to the V600E B-RAF mutation (5). WM-266-4 xenografts were chosen for this study because they are moderately responsive to MEK inhibition allowing for enough tumor tissue to remain after 14 days of dosing to evaluate both GDC-0973 concentrations and PD response in tumor. Little or no tumor tissue remains following 14 days of dosing in xenograft mice bearing more sensitive melanoma tumors such as A375. The plasma and tumor concentration–time profiles and tumor %pERK decrease for the WM-266-4 xenografts given a single or multiple daily oral doses of 1, 3, and 10 mg/kg of GDC-0973 are presented in Fig. 2A and B, respectively. Following single oral doses, GDC-0973 concentrations and PD response is dose-dependent (Fig. 2A; Supplementary Fig. S2). GDC-0973 concentrations in tumor tissue are both higher and more sustained than in plasma. PD response mirrored tumor concentrations with %pERK decrease in tumor observed well beyond the time frame that GDC-0973 was observed in plasma. Overall, a similar situation was observed following 14 days of daily GDC-0973 dosing. However, despite higher GDC-0973 concentrations in plasma and tumor due to drug accumulation than in the single dose study, the magnitude of tumor %pERK decrease was less at later time points (Fig. 2B).

Published OnlineFirst April 10, 2012; DOI: 10.1158/1078-0432.CCR-12-0445

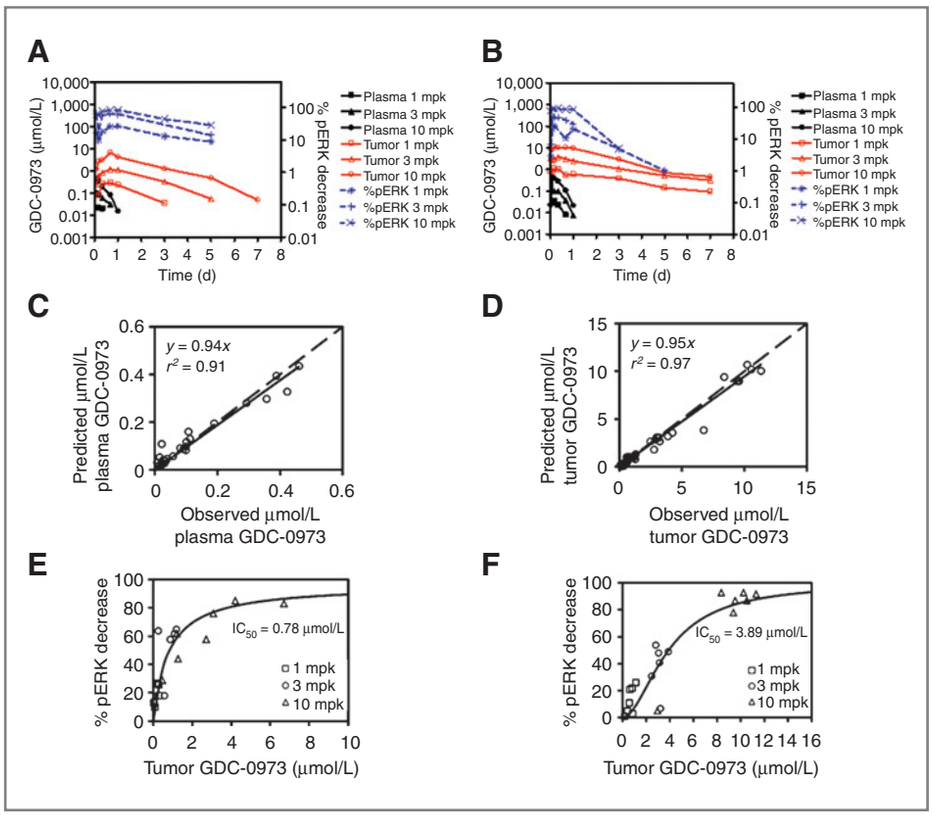

Figure 2. GDC-0973 plasma and tumor concentration and tumor %pERK decrease profiles in WM-266-4 xenografts following oral administration of a single (A) or multiple (B) oral doses of GDC-0973 at 1, 3, and 10 mg/kg (mpk). For A, the time on the *x*-axis refers to time after the first dose and for B, the time on the *x*-axis refers to the time after the last (14th) dose. Each point in A and B represents the mean of 3 animals. Plots of the observed versus predicted GDC-0973 plasma (C) and tumor (D) concentrations following fitting of WM-266-4 xenograft data to the PK model presented in Fig. 1A. In C and D, the dashed line is the line of identity and the solid line is a regression line. Plots of the relationship between GDC-0973 tumor concentration and tumor %pERK decrease from single (E) or multiple dose (F) studies of GDC-0973 in WM-266-4 xenograft mice. In E and F, the solid line is predicted tumor %pERK decrease from the PK–PD model shown in Fig. 1B.

Figure 2C and D shows plots of observed versus predicted plasma and tumor GDC-0973 concentrations, respectively, following simultaneous fitting of the PK model (Fig. 1A) to single and multiple dose PK data from WM-266-4 xenografts. Estimated PK parameters are presented in Table 1.

Table 1. Summary of PK and PD parameters estimated from WM-266-4 xenograft studies

PK parameter	Estimate (%SE)[a]	
k_a, h^{-1}	1.08 (5.6)	
Cl, L/h/kg	3.13 (2.1)	
Cl_{pt}, L/h/kg	1.74 (4.5)	
Cl_{tp}, L/h/kg	0.040 (5.8)	
V/F, L/kg	40.5 (1.5)	
PD parameter for %pERK decrease	**Single dose estimate (%SE)[a]**	**Multiple dose estimate (%SE)[a]**
IC_{50}, μmol/L	0.78 (26.4)	3.89 (7.7)
I_{max} (%)	97 (10.4)	100 (fixed)
h	1 (fixed)	1.85 (13.8)

[a]Fitted parameters are expressed as estimate followed by the %SE in parentheses.

The higher and sustained tumor concentrations observed in WM-266-4 xenografts was reflected in the estimate of intercompartmental clearance from the plasma to tumor compartment (Cl_{pt}) being approximately 40-fold higher than the intercompartmental clearance from the tumor to plasma compartment (Cl_{tp}). PD parameters describing pERK reduction were also estimated separately for single and multiple dose experiments using the PK–PD model (Fig. 1B). Plots showing observed and model-predicted %pERK decrease in tumor are presented in Fig. 2E and F for single and multiple dose studies, respectively. No evidence of hysteresis indicative of time delays in onset of PD response was observed in these plots. Associated PD parameter estimates for single and multiple dose studies are presented in Table 1. On the basis of the PD parameters presented in Table 1, there appeared to be a shift in the *in vivo* potency of GDC-0973 following multiple days of dosing with the %pERK decrease IC_{50} estimate increasing from 0.78 to 3.89 μmol/L. PK and PD parameters were estimated with good precision with %SE for all parameters shown in Table 1 being less than 30%. Overall, the proposed PK–PD model adequately characterized the plasma and tumor concentrations and tumor pERK inhibition in WM-266-4 xenografts.

Human simulations identify minimum GDC-0973 target plasma concentrations and predict tumor PD response and active doses. One of the primary objectives of the WM-266-4 xenograft studies was to characterize the relationship

Published OnlineFirst April 10, 2012; DOI: 10.1158/1078-0432.CCR-12-0445

between plasma concentrations and tumor PD modulation to identify a minimum target plasma concentration required in patients. Early reports of the phase I trial for the MEK inhibitor PD-0325901 suggested a trend toward progression-free survival at %pERK decreases of more than 60% (19). In addition, signs of activity were observed in the phase I clinical trial for CI-1040, a first-generation MEK1/2 inhibitor, at doses associated with a median tumor %pERK decrease of 73% (20). On the basis of these data, we set ≥80% pERK decrease at steady state as our target for tumor PD modulation.

The PK model used to characterize tumor disposition in WM-266-4 xenograft mice (Fig. 1A) was fit to mean GDC-0973 plasma concentration–time data from the first cohort of patients on the GDC-0973 phase I clinical trial (16). An assumption was made that tumor disposition is similar in humans and xenograft-bearing mice; therefore, Cl_{tp} and Cl_{pt} were fixed to estimates from WM-266-4 xenograft mice during the fitting process. The estimated human PK parameters are presented in Supplementary Table S1, and the plot of observed versus predicted GDC-0973 plasma concentrations following the model fitting is shown in Supplementary Fig. S3. Simulations were conducted using the human PK and PD parameters from the WM-266-4 single dose study. The PD parameters from the single dose WM-266-4 study were chosen for this simulation because we wanted to identify the minimum target plasma concentration, and the *in vivo* IC_{50} following multiple doses of GDC-0973 was approximately 5-fold higher (see Table 1). In addition, the *in vivo* IC_{50} estimate from the single dose WM-266-4 study was comparable with the *in vivo* IC_{50} estimate from V600E B-RAF mutant A375 melanoma xenograft mice (see below). On the basis of the human simulation shown in Fig. 3A, the minimum GDC-0973 plasma concentration at trough (24 hours postdose) required for ≥80% tumor pERK decrease at steady state is 83 nmol/L. No adjustments were made to account for potential differences in free drug concentrations because there is no evidence of GDC-0973 protein–binding differences in mouse and human plasma (both ∼95% bound, data not shown).

To assess the cohort at which the target of ≥80% tumor pERK decrease could be achieved, we conducted prospective human simulations of the phase I clinical trial. Figure 3B and C shows prospective human trial simulations mimicking the planned doses in the phase I clinical trial. Because we would not know the B-RAF mutation status in patients during the dose-escalation portion of the phase I clinical trial, we conducted these prospective human simulations using PD parameters from both the single and multiple dose GDC-0973 studies in WM-266-4 xenograft mice to provide a range of doses where we might see antitumor activity. On the basis of our simulations, the goal of reducing pERK by ≥80% could be achieved at a daily oral dose of 28 (0.4 mg/kg; shown in Fig. 3B) to 112 mg (1.6 mg/kg; shown in Fig. 3C) of GDC-0973 in cohorts 4 to 6 of the clinical trial.

During the course of the phase I clinical trial, tumor biopsies were collected for biomarker assessments. To test the performance of our PK–PD model, we conducted a retrospective simulation to compare the modeled decrease in tumor pERK with the observed immunohistochemistry-assessed decrease in one patient from the 0.2-mg/kg dose cohort for whom we had evaluable pre- and postdosing matched tumor biopsies. Two tumor biopsies were collected from this patient at 4 hours postdose on day 20 of dosing. Human simulations at the same dose (0.2 mg/kg) using PD parameters from both single and multiple dose WM-266-4

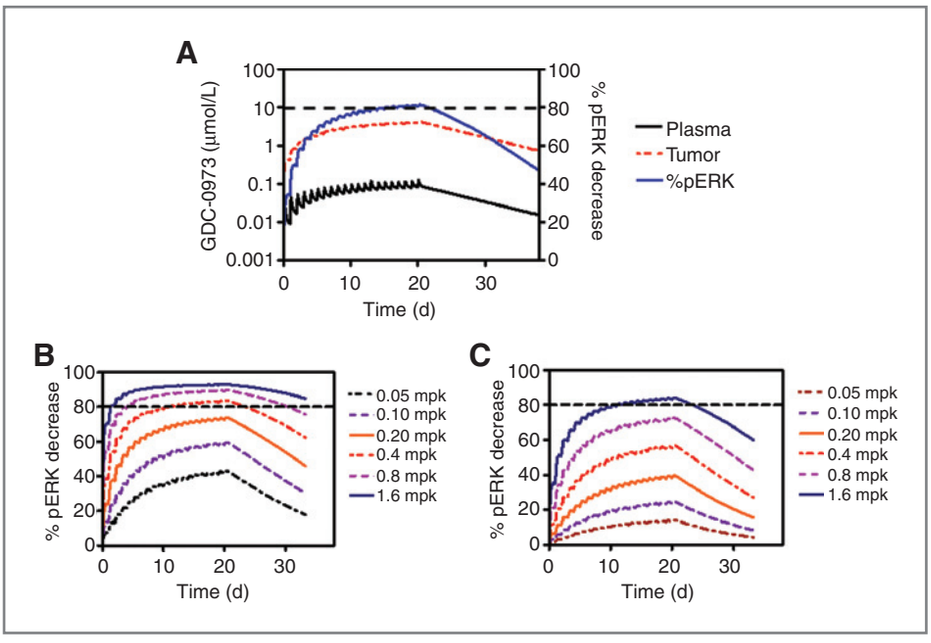

Figure 3. Human simulation of GDC-0973 plasma and tumor concentrations and tumor %pERK decrease at a dose (0.33 mg/kg) where tumor %pERK decrease is ≥80% at steady state (A). B and C, human simulations of tumor %pERK decrease for escalating daily doses of GDC-0973 using single (B) or multiple dose (C) PD parameters from WM-266-4 xenograft studies. The horizontal black dashed line in A to C serves as a reference line for 80% pERK decrease in tumor.

Published OnlineFirst April 10, 2012; DOI: 10.1158/1078-0432.CCR-12-0445

studies resulted in a mean tumor pERK decrease of 51% (29% using multiple dose PD parameters and 73% using single dose PD parameters) comparable with the observed mean decrease of 41% (29% and 52% in independent metastatic lesions; Genentech, unpublished data).

Studies in A375 xenografts

Relationship between tumor %pERK decrease and GDC-0973 tumor concentrations in A375 xenograft mice. To understand the relationship between GDC-0973 concentration and PD response in an additional B-RAF mutant xenograft tumor, Equation (D) was fit to GDC-0973 tumor concentration and tumor pERK data from A375 xenograft–bearing mice. A375 melanoma cells harbor the B-RAF V600E mutation conferring activation of the RAF/MEK/ERK pathway (5, 21). This V600E mutant melanoma cell line is relevant for understanding the effect of MEK inhibition on human patients with melanoma with this common B-RAF mutation. The *in vivo* IC_{50} estimated in A375 xenograft mice (0.52 μmol/L; see Fig. 4A) was comparable with the *in vivo* IC_{50} estimated from the single dose WM-266-4 xenograft study (i.e., 0.78 μmol/L; see Table 1 and Fig. 2E).

GDC-0973 shows dose-dependent antitumor efficacy in A375 xenograft mice. The objective of the A375 xenograft efficacy study was to characterize the antitumor activity of GDC-0973 in xenograft mice bearing melanoma tumors with the V600E B-RAF mutation. GDC-0973 showed dose-dependent inhibition of tumor growth following oral

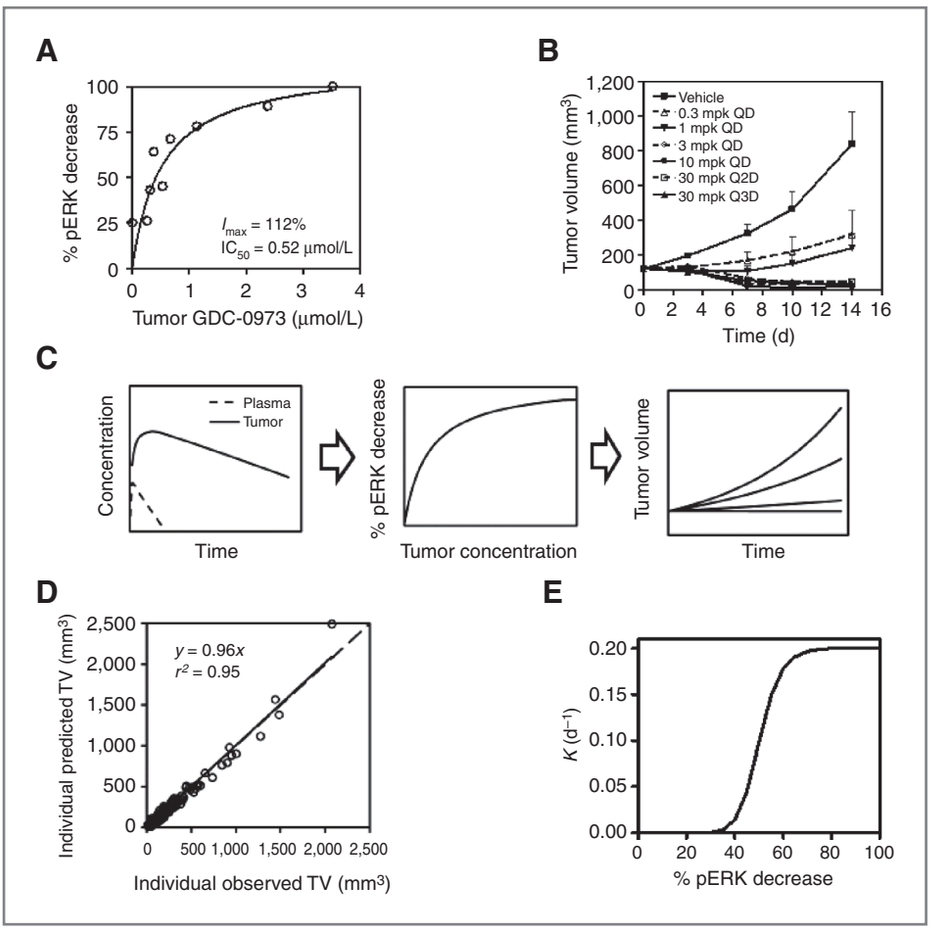

Figure 4. A plot of the relationship between GDC-0973 tumor concentration and tumor %pERK decrease following oral administration of a single dose of GDC-0973 to A375 xenografts (A). The solid line in A is the model predicted %pERK decrease, and model estimates of I_{max} and IC_{50} are presented. *In vivo* efficacy of GDC-0973 in A375 xenografts is presented in B. In B, QD represents once daily, Q2D represents once every 2 days, and Q3D represents once every 3 days. C, the integrated PK–PD-efficacy analysis used to relate pathway modulation to antitumor efficacy. The analysis involves first linking plasma to tumor concentrations and then tumor concentrations to tumor %pERK decrease in A375 xenograft mice using the model described in Fig. 1B such that tumor %pERK decrease can be simulated for all dosing regimens in the xenograft efficacy study. The final step of the analysis involves understanding the relationship between tumor %pERK decrease and antitumor efficacy using the full integrated PK–PD-efficacy model shown in Fig. 1C where tumor %pERK decrease drives antitumor effect. D, a plot of individual observed versus individual predicted tumor volumes from the A375 xenograft efficacy study following fitting the integrated PK–PD-efficacy model to tumor volume data. E, a plot showing the relationship between % pERK decrease in tumor and rate constant (K) describing the antitumor effect of GDC-0973 in A375 xenograft mice. Parameters used to simulate (E) are as follows: $K_{max} = 0.201\ day^{-1}$, $K(\%I)_{50}$ = 50.2% pERK decrease, and n = 11.5.

Published OnlineFirst April 10, 2012; DOI: 10.1158/1078-0432.CCR-12-0445

administration over a broad dose range (0.3–30 mg/kg) and using varying schedules (once daily, every 2 days, and every 3 days; see Fig. 4B). All 3 schedules provided significant antitumor activity in this model, consistent with published reports for GDC-0973 (15).

Integrated PK–PD-efficacy analysis in A375 xenografts. An integrated PK–PD-efficacy analysis was conducted on the A375 xenograft efficacy study to understand the relationship between modulation of the RAF/MEK/ERK signaling pathway and antitumor efficacy in a B-RAF V600E melanoma tumor model. All 70 xenograft mice (10 per dose group) were included in the analysis. The process is described in Fig. 4C and uses the integrated PK–PD-efficacy model shown in Fig. 1C. In brief, a PK–PD model (Fig. 1B) built using the PK parameters from WM-266-4 xenografts (Table 1) and PD parameters from A375 xenografts (Fig. 4A) was used to simulate tumor %pERK decreases for all dosing regimens in the A375 xenograft efficacy study. Individual longitudinal tumor volume data from all A375 xenograft–bearing mice were fit simultaneously to an integrated PK–PD-efficacy model (Fig. 1C) which involved the addition of an indirect response model [Equation (E)], where tumor growth inhibition is driven by tumor %pERK decrease, to the PK–PD model described. Figure 4D is a plot of the individual observed versus individual predicted tumor volumes of the resulting population model fit, suggesting that the model adequately captured the growth characteristics of the tumor data from the efficacy study. Estimated PD parameters from this integrated PK–PD-efficacy analysis are presented in Table 2. PD parameters along with the inter- and intraindividual variability were estimated with acceptable precision with %SE of all estimates being $\leq$38%. The maximum antitumor effect (K_{max}) was approximately 2-fold larger than the estimated net growth rate constant (k_{ng}) consistent with regression of A375 xenograft tumors in response to GDC-0973 treatment.

Table 2. A375 melanoma xenograft PD parameter estimates from integrated population PK–PD-efficacy model

Parameter	Population mean (%SE)	Interindividual variance (%SE)
k_{ng}, d^{-1}	0.0828 (10.7)	0.426 (26.9)
K_{max}, d^{-1}	0.201 (0.4)	Fixed
K $(\%I)_{50}$ (%pERK decrease)	50.2 (0.7)	Fixed
n	11.5 (0.4)	Fixed
Initial tumor volume, mm^3	117 (3.1)	0.024 (37.6)
Residual variability		
Proportional error σ_{prop} (%)	0.113 (19.3)	—
Additive error σ_{add} (mm^3)	15.2 (14.8)	—

Using the estimated PD parameters, a plot of the relationship between RAF/MEK/ERK pathway knockdown (i.e., %pERK decrease) and efficacy (i.e., K is the rate constant describing the antitumor effect of GDC-0973) was generated and is shown in Fig. 4E. The steep relationship between pathway inhibition and efficacy is characterized by a Hill slope (n) of approximately 11 (Fig. 4E, Table 2) and suggests that there is a pathway suppression threshold beyond which antitumor activity "switches on." In addition, the plot shown in Fig. 4E suggests that for maximal antitumor activity, more than 60% to 70% %pERK decrease is required in A375 xenografts.

Discussion

GDC-0973 is a potent and selective MEK1 inhibitor that is currently in phase I clinical trials as a potential antitumor agent. The current study shows that GDC-0973 causes potent inhibition of pERK in 2 preclinical models of B-RAF mutant melanoma, WM-266-4 and A375 xenograft mice. A375 xenografts bear melanoma tumors that harbor a V600E B-RAF mutation that is sensitive to MEK inhibition and represents a common mutation in human patients with melanoma (5, 21). In contrast, WM-266-4 (V600D B-RAF mutation and PTEN-deficient) xenografts are only moderately responsive to MEK inhibition but allow for sufficient tumor tissue after multiple days of GDC-0973 dosing required to characterize GDC-0973 tumor disposition. Our studies with WM-266-4 xenografts show that GDC-0973 is not only present at higher concentrations in tumor relative to plasma but also resides in the tumor for a longer duration. *In vivo* IC_{50} values based on GDC-0973 concentrations in tumor tissue (A375 and WM-266-4 xenografts) ranged from 0.52 to 3.89 μmol/L, and the PD response was shown to be directly correlated with tumor concentrations in both xenograft models examined. These data are consistent with our observations from preliminary studies in other xenograft mice (data not shown).

Mechanistic PK–PD modeling serves as an important tool to bridge the gap between preclinical and clinical data (22–24). Our studies used WM-266-4 xenograft–bearing mice as an experimental system to characterize the GDC-0973 concentration in tumor tissue over time. The incorporation of human PK into the PK–PD model built using WM-266-4 xenograft mice studies allows for normalization of known species differences in PK (25). We chose a sustained pERK reduction target of $\geq$80% at steady state as the PD endpoint for these simulations based on early published reports on MEK inhibitors in the clinic (19, 20). Our simulations using this "human PK–PD model" identified a minimum plasma concentration of 83 nmol/L where we anticipated that $\geq$80% pERK decrease would be maintained at steady state in tumor tissues. Prospective simulations of a human dose escalation mimicking the phase I trial design predicted that doses of 28 to 112 mg once daily would be sufficient to meet this target. Antitumor activity in patients with melanoma

Published OnlineFirst April 10, 2012; DOI: 10.1158/1078-0432.CCR-12-0445

with B-RAF mutations has now been reported at daily doses of 60 and 100 mg in the clinic (16), consistent with predictions based on the described PK–PD model.

One interesting observation was that the tumor GDC-0973 concentration required to reduce pERK in WM-266-4 tumor tissue increased during the 2-week dosing period. The reasons for this shift in sensitivity over time are not known but could be explained by subpopulations of less sensitive tumor cells escaping MEK inhibition or the emergence of resistant cells in response to continuous MEK inhibition. Both mechanisms of resistance have been reported for B-RAF and MEK inhibitors (26–28)

As a final part of our analysis, we wanted to quantify the relationship between RAF/MEK/ERK pathway modulation (%pERK decrease) and tumor growth inhibition through the use of an integrated PK–PD-efficacy model (Fig. 1C). A "pathway modulation–response curve" showing the relationship between %pERK decrease and *K* (a measure of antitumor effect of GDC-0973) was sigmoidal and described by a Hill coefficient of approximately 11 (Fig. 4E). This steep relationship between pathway modulation and antitumor effect is suggestive of a threshold of pERK inhibition beyond which antitumor activity "turns on." The observed "switch-like" behavior is consistent with reports of ultrasensitive stimulus–response curves observed for MAPK cascades (29). "Switch-like" behavior has also been recently reported in similar analyses conducted with other kinase inhibitors such as GDC-0879, a B-RAF kinase inhibitor (30), and GDC-0834, a Bruton's tyrosine kinase inhibitor (31), and the hedgehog signaling pathway inhibitor, vismodegib (32).

Robust clinical activity has been reported for vemurafenib (PLX4032) in patients with B-RAF mutant melanoma (12, 33). Interestingly, no clinical responses were reported in patients with melanoma with cytoplasmic reductions of pERK in tumor of less than approximately 60%, whereas pERK reductions were typically more than 80% in patients who responded to vemurafenib (33). Similarly, phase I data for PD-0325901, an MEK inhibitor, showed signs of clinical activity in patients with B-RAF V600E melanoma at pERK decreases of 76% or greater (10). On the basis of human simulations presented in the manuscript, the %pERK decrease in tumor tissue is anticipated to be more than 80% at clinical doses of 28 to 112 mg/d GDC-0973, consistent with the observed clinical activity in patients with B-RAF mutant melanoma at daily doses of 60 and 100 mg (16). Taken together, available clinical data suggest that a high degree of suppression of the RAF/MEK/ERK pathway, above a certain threshold, is required for robust antitumor activity.

Preclinical PK–PD modeling of anticancer therapeutics is associated with certain assumptions and caveats. Xenograft mouse models are the most common preclinical *in vivo* efficacy models used to evaluate and select new anticancer therapies for clinical development (34, 35). An important assumption when translating xenograft data to humans is that drug concentrations required for PD modulation and antitumor activity are the same in xenograft-bearing mice and human patients with cancer. This assumes that drug distribution is similar, despite reported differences in tumor vasculature and transport in xenograft versus human tumors (36). Also, differences in growth rate of human and xenograft tumors complicate the interpretation of xenograft data. Finally, the selection of relevant tumor types that are reflective of the disease that is being targeted is challenging. Despite these challenges, the present GDC-0973 study illustrates how PK–PD modeling can be used to improve clinical translation of preclinical data to humans through integration of all available information. Through our PK–PD analysis using combined preclinical and limited early clinical data, we characterized the relationship between GDC-0973 plasma and tumor concentrations, tumor PD response and antitumor activity. Using this knowledge, we were able to successfully prospectively predict active doses of GDC-0973 in patients with V600E melanoma and roughly identify the number of dose escalations in the phase I clinical trial required to reach active doses.

Disclosure of Potential Conflicts of Interest

B.T. Aftab has ownership interest (including patents) in Exelixis. No potential conflicts of interest were disclosed by the other authors.

Authors' Contributions

Conception and design: H. Wong, L. Vernillet, A. Peterson, J.-F. Martini, E.F. Choo, R. Aoyama, J. Prescott

Development of methodology: H. Wong, L. Vernillet, P. Yu, C. Li, Y. Shi, S. Lam

Acquisition of data (provided animals, acquired and managed patients, provided facilities, etc.): L. Vernillet, J.A. Ware, L. Lee, J.-F. Martini, P. Yu, G. Del Rosario, K.P. Hoeflich, B.T. Aftab, R. Aoyama, S. Lam

Analysis and interpretation of data (e.g., statistical analysis, biostatistics, computational analysis): H. Wong, L. Vernillet, A. Peterson, J.A. Ware, J.-F. Martini, P. Yu, K.P. Hoeflich, B.T. Aftab, R. Aoyama, S. Lam

Writing, review, and/or revision of the manuscript: H. Wong, L. Vernillet, A. Peterson, J.-F. Martini, P. Yu, E.F. Choo, K.P. Hoeflich, M. Belvin, J. Prescott

Administrative, technical, or material support (i.e., reporting or organizing data, constructing databases): P. Yu, G. Del Rosario, B.T. Aftab

Study supervision: A. Peterson, J.-F. Martini, P. Yu, K.P. Hoeflich, R. Aoyama, J. Prescott

Acknowledgments

The authors thank colleagues at Exelixis and Genentech for their contributions in generating data for this study. The authors also thank Drs. Stephen E. Gould, Mark Merchant, O. Helen Chan, Lichuan Liu, and Cornelis Hop for their helpful comments and discussion.

Received February 8, 2012; revised March 21, 2012; accepted March 30, 2012; published OnlineFirst April 10, 2012.

References

1. Sebolt-Leopold JS, Herrera R. Targeting the mitogen-activated protein kinase cascade to treat cancer. Nat Rev Cancer 2004;4:937–47.
2. McCubrey JA, Steelman LS, Chappell WH, Abrams SL, Wong EW, Chang F, et al. Roles of the Raf/MEK/ERK pathway in cell growth, malignant transformation and drug resistance. Biochim Biophys Acta 2007;1773:1263–84.
3. Friday BB, Adjei AA. Advances in targeting the Ras/Raf/MEK/Erk mitogen-activated protein kinase cascade with MEK

Published OnlineFirst April 10, 2012; DOI: 10.1158/1078-0432.CCR-12-0445

inhibitors for cancer therapy. Clin Cancer Res 2008;14:342–6.
4. Chapman MS, Miner JN. Novel mitogen-activated protein kinase kinase inhibitors. Expert Opin Investig Drugs 2011;20:209–20
5. Davies H, Bignell GR, Cox C, Stephens P, Edkins S, Clegg S, et al. Mutations of the BRAF gene in human cancer. Nature 2002;417:949–54.
6. Yuen ST, Davies H, Chan TL, Ho JW, Bignell GR, Cox C, et al. Similarity of the phenotypic patterns associated with BRAF and KRAS mutations in colorectal neoplasia. Cancer Res 2002;62:6451–5
7. Li N, Batt D, Warmuth M. B-Raf kinase inhibitors for cancer treatment. Curr Opin Investig Drugs 2007;8:452–6.
8. Mercer KE, Pritchard CA. Raf proteins and cancer: B-Raf is identified as a mutational target. Biochim Biophys Acta 2003;1653:25–40.
9. Solit DB, Garraway LA, Pratilas CA, Sawai A, Getz G, Basso A, et al. BRAF mutation predicts sensitivity to MEK inhibition. Nature 2006;439:358–62
10. LoRusso PM, Krishnamurthi SS, Rinehart JJ, Nabell LM, Malburg L, Chapman PB, et al. Phase I pharmacokinetic and pharmacodynamic study of the oral MAPK/ERK kinase inhibitor PD-0325901 in patients with advanced cancers. Clin Cancer Res 2010;16:1924–37.
11. Banerji U, Camidge DR, Verheul HM, Agarwal R, Sarker D, Kaye SB, et al. The first-in-human study of the hydrogen sulfate (Hyd-sulfate) capsule of the MEK1/2 inhibitor AZD6244 (ARRY-142886): a phase I open-label multicenter trial in patients with advanced cancer. Clin Cancer Res 2010;16:1613–1623.
12. Flaherty KT, Puzanov I, Kim KB, Ribas A, McArthur GA, Sosman JA, et al. Inhibition of mutated, activated BRAF in metastatic melanoma. N Engl J Med 2010;363:809–19
13. Corcoran RB, Settleman J, Engelman JA. Potential therapeutic strategies to overcome acquired resistance to BRAF or MEK inhibitors in BRAF mutant cancers. Oncotarget 2011;2:336–46
14. Poulikakos PI, Solit DB. Resistance to MEK inhibitors: should we target upstream? Sci Signal 2011;4:pe16.
15. Hoeflich KP, Merchant M, Orr C, Chan J, Den Otter D, Berry L, et al. Intermittent administration of MEK inhibitor GDC-0973 plus PI3K inhibitor GDC-0941 triggers robust apoptosis and tumor growth inhibition. Cancer Res 2012;72:210–9.
16. Rosen L, LoRusso P, Ma WW, Goldman J, Weise A, Colevas A, et al. A first-in-human phase 1 study to evaluate the MEK1/2 inhibitor GDC-0973 administered daily in patients with advanced solid tumors [abstract]. In: Proceedings of the 102nd Annual Meeting of the American Association for Cancer Research; 2011 Apr 2–6; Orlando, FL. Philadelphia (PA): AACR; 2011.Abstract nr 4716.
17. Bauer RJ, Guzy S. Monte Carlo parametric expectation maximization (MC-PEM) method for analyzing population pharmacokinetic/pharmacodynamic (PK/PD) data. In:D'Argenio DZ, editor. Advanced methods of pharmacokinetic and pharmacodynamic system analysis. Boston, MA: Kluwer; 2004. p. 135–63.
18. D'Argenio DZ, Schumitzky A. ADAPT II user's guide: pharmacokinetic/pharmacodynamic systems analysis software. Los Angeles, CA: Biomedical Simulations Resource; 1997.
19. Tan W, DePrimo SE, Krishnamurthi SS, Rinehart JJ, Nabell LM, Nickens D, et al. Pharmacokinetic (PK) and pharmacodynamic (PD) results of a phase I study of PD-0325901, a second generation oral MEK inhibitor, in patients with advanced cancer. Mol Cancer Ther 2007;6:3648s. Abstract nr B109.
20. LoRusso PM, Adjei AA, Varterasian M, Gadgeel S, Reid J, Mitchell DY, et al. Phase I and pharmacodynamic study of the oral MEK inhibitor CI-1040 in patients with advanced malignancies. J Clin Oncol 2005;23:5281–93.
21. Wan PT, Garnett MJ, Roe SM, Lee S, Niculescu-Duvaz D, Good VM, et al. Mechanism of activation of the RAF-ERK signaling pathway by oncogenic mutations of B-RAF. Cell 2004;116:855–67.
22. Mager DE, Wyska E, Jusko WJ. Diversity of mechanism-based pharmacodynamic models. Drug Metab Dispos 2003;31:510–8.
23. Yamazaki S, Skaptason J, Romero D, Lee JH, Zou HY, Christensen JG, et al. Pharmacokinetic-pharmacodynamic modeling of biomarker response and tumor growth inhibition to an orally available cMet kinase inhibitor in human tumor xenograft mouse models. Drug Metab Dispos 2008;36:1267–74
24. Tanaka C, O'Reilly T, Kovarik JM, Shand N, Hazell K, Judson I, et al. Identifying optimal biologic doses of everolimus (RAD001) in patients with cancer based on the modeling of preclinical and clinical pharmacokinetic and pharmacodynamic data. J Clin Oncol 2008;26:1596–602.
25. Lin JH. Species similarities and differences in pharmacokinetics. Drug Metab Dispos 1995;23:1008–21
26. Emery CM, Vijayendran KG, Zipser MC, Sawyer AM, Niu L, Kim JJ, et al. MEK1 mutations confer resistance to MEK and B-RAF inhibition. Proc Natl Acad Sci U S A 2009;106:20411–6.
27. Corcoran RB, Dias-Santagata D, Bergethon K, Iafrate AJ, Settleman J, Engelman JA. BRAF gene amplification can promote acquired resistance to MEK inhibitors in cancer cells harboring the BRAF V600E mutation. Sci Signal 2010;3:ra84.
28. Paraiso KH, Fedorenko IV, Cantini LP, Munko AC, Hall M, Sondak VK, et al. Recovery of phospho-ERK activity allows melanoma cells to escape from BRAF inhibitor therapy. Br J Cancer 2010;102:1724–30.
29. Huang CY, Ferrell JE Jr. Ultrasensitivity in the mitogen-activated protein kinase cascade. Proc Natl Acad Sci U S A 1996;93:10078–83.
30. Wong H, Belvin M, Herter S, Hoeflich KP, Murray LJ, Wong L, et al. Pharmacodynamics of 2-{4-[(1E)-1-(hydroxyimino)-2,3-dihydro-1H-inden-5-yl]-3-(pyridine-4-yl)-1H-pyrazol-1-yl}ethan-1-ol (GDC-0879), a potent and selective B-Raf kinase inhibitor: relationships between systemic concentrations, pMEK1 inhibition, and efficacy. J Pharmacol Exp Ther 2009;329:360–7.
31. Liu L, Di Paolo J, Barbosa J, Rong H, Reif K, Wong H. Anti-arthritis effect of a novel Bruton's tyrosine kinase inhibitor in rat collagen-induced arthritis and mechanism-based pharmacokinetic/pharmacodynamic modeling: relationships between inhibition of BTK phosphorylation and efficacy. J Pharmacol and Exp Ther 2011;338:154–63.
32. Wong H, Alicke B, West K, Pacheco P, La H, Januario T, et al. Relationship between hedgehog pathway modulation and anti-tumor effect in preclinical models of mutational and ligand-driven tumors: a pharmacokinetic-pharmacodynamic analysis using vismodegib. Clin Canc Res 2011;17:4682–92.
33. Bollag G, Hirth P, Tsai J, Zhang J, Ibrahim PN, Cho H, et al. Clinical efficacy of a RAF inhibitor needs broad target blockade in BRAF-mutant melanoma. Nature 2010;467:596–9.
34. Kelland LR. Of mice and men: values and liabilities of the athymic nude mouse model in anticancer drug development. Eur J Cancer 2004;40:827–36.
35. Teicher BA. Tumor models for efficacy determination. Mol Cancer Ther 2006;5:2435–43.
36. Jang SH, Wientjes MG, Lu D, Au JL. Drug delivery and transport to solid tumors. Pharm Res 2003;20:1337–50.

AACR American Association for Cancer Research

Clinical Cancer Research

Bridging the Gap between Preclinical and Clinical Studies Using Pharmacokinetic–Pharmacodynamic Modeling: An Analysis of GDC-0973, a MEK Inhibitor

Harvey Wong, Laurent Vernillet, Amy Peterson, et al.

Clin Cancer Res 2012;18:3090-3099. Published OnlineFirst April 10, 2012.